Artificial Upwelling - A New Narrative

Malte Jürchott[1], Andreas Oschlies[2], and Wolfgang Koeve[2]

[1]GEOMAR Helmholtz Centre for Ocean Research Kiel
[2]Helmholtz-Zentrum für Ozeanforschung Kiel, GEOMAR

December 22, 2022

Abstract

The current narrative of artificial upwelling (AU) is to use ocean pipes to pump nutrient rich deep water to the ocean surface, thereby stimulating the biological carbon pump. This simplistic concept of AU does not take the response of the solubility pump or the CO_2 emission scenario into account. Using global ocean-atmosphere model experiments and several idealized model tracers we show that the effectiveness of almost globally applied AU from the year 2020 to 2100 to draw down CO_2 from the atmosphere is strongly dependent on the CO_2 emission scenario and ranges from 1.01 Pg C / year under RCP 8.5 to 0.32 Pg C / year under RCP 2.6. The solubility pump becomes equally effective compared to the biological carbon pump under the highest emission scenario (RCP 8.5), but responds with CO_2 outgassing under low CO_2emission scenarios.

Artificial Upwelling – A New Narrative

Jürchott, M.[1], Oschlies, A.[1], Koeve, W.[1]

[1]GEOMAR Helmholtz Centre for Ocean Research Kiel, Germany

Key Points:

- Artificial Upwelling effectiveness to draw down CO_2 from the atmosphere is strongly dependent on the future CO_2 emission scenario.
- The solubility pump becomes as effective as the biological carbon pump under high emission scenarios.
- Organic matter transfer efficiency decreases under artificial upwelling, likely due to higher water temperatures below the ocean's surface.

Keywords:

carbon dioxide removal method, artificial upwelling, biological carbon pump, solubility pump, emission scenarios, UVic ESM

Corresponding Author: Malte Jürchott, mjuerchott@geomar.de

Abstract

The current narrative of artificial upwelling (AU) is to use ocean pipes to pump nutrient rich deep water to the ocean surface, thereby stimulating the biological carbon pump. This simplistic concept of AU does not take the response of the solubility pump or the CO_2 emission scenario into account. Using global ocean-atmosphere model experiments and several idealized model tracers we show that the effectiveness of almost globally applied AU from the year 2020 to 2100 to draw down CO_2 from the atmosphere is strongly dependent on the CO_2 emission scenario and ranges from 1.01 Pg C / year under RCP 8.5 to 0.32 Pg C / year under RCP 2.6. The solubility pump becomes equally effective compared to the biological carbon pump under the highest emission scenario (RCP 8.5), but responds with CO_2 outgassing under low CO_2 emission scenarios.

Plain Language Summary

Artificial upwelling (AU) is a proposed marine carbon dioxide removal (CDR) method, which suggests deploying pipes in the ocean to pump deep water to the ocean's surface. This process theoretically has several different impacts on the surface layer including an increase in the nutrient concentration, as well as a decrease in surface water temperature. Changes in the carbon cycle and associated with biological components are covered by the biological carbon pump, while changes via physical-chemical processes are covered by the solubility pump. Using numerical ocean modeling and simulating almost globally applied AU between the years 2020 and 2100 under several different atmospheric CO_2 emission scenarios, we show that AU leads under every simulated emission scenario to an additional CO_2 uptake of the ocean, but the potential increases under higher emission scenarios (up to 1.01 Pg C / year under RCP 8.5). The individual contribution via the biological carbon pump is under every emission scenario positive, while the processes associated with the solubility pump can lead to CO_2 uptake under higher emission scenarios and CO_2 outgassing under lower emission scenarios.

1 Introduction

Earths' atmospheric CO_2 concentration (pCO_2^{atm}) has strongly increased since preindustrial times and continues to rise despite considerable CO_2 emission reduction efforts (IPCC, 2018). Even when optimistically assuming that humanity ambitiously intensifies emission reduction efforts, we still have to

deal with hard-to-abate CO_2 emissions (Thoni et al., 2020). To compensate these residual emissions and reach a net zero carbon emission world around mid century, we likely need to actively remove CO_2 from the atmosphere, which has led to an increased interest in carbon dioxide removal (CDR) technologies (GESAMP, 2019).

One proposed marine CDR idea is to use artificial upwelling (AU) to pump up nutrients from the interior ocean to the sea surface via ocean pipes to stimulate the biological carbon pump (Lovelock & Rapley, 2007). This process is supposed to enhance primary production at the sea surface, thereby increase export production and finally lead to a net CO_2 flux from the atmosphere into the interior ocean. Several studies have already shown that this simplistic view of stimulating the biological carbon pump (Volk & Hoffert, 1985) via AU is not sufficient for a comprehensive evaluation of this technology in terms of its carbon drawdown potential and its climate effects (Dutreuil et al., 2009; Yool et al., 2009; Oschlies et al., 2010; Keller et al., 2014). Especially pumping up water with a high concentration of dissolved inorganic carbon (DIC) may even lead to a net CO_2 outgassing despite an increase in export production (Dutreuil et al., 2009). One may be tempted to argue that AU in a fixed C-N-P stoichiometry ("Redfield") world model should result in a net zero carbon uptake through the biological carbon pump. However, pumping up preformed nutrients (Duteil et al., 2012) to the sea surface may contribute to an additional carbon uptake. AU will also affect properties such as alkalinity, sea surface temperature and preformed DIC, which collectively may cause a response of the solubility pump (Volk & Hoffert, 1985) with the potential to influence the atmosphere to ocean carbon flux too. Also the dependence of the CO_2-uptake due to AU on the pCO_2 path (the assumption of the underlying CO_2 emission scenario) under which it takes place is not well understood.

To get a better understanding of the effects of AU and the processes involved, we simulate AU in an Earth System model of intermediate complexity combined with an idealized tracer approach and under a range of CO_2 emission scenarios to (i) evaluate the general impact of AU on the ocean's carbon uptake under different CO_2 emission scenarios, (ii) to explicitly quantify the respective importance of the biological carbon pump and the solubility pump in the model simulations, and (iii) to identify the important carbon uptake, release and storage regions in the ocean.

2 Methods

2.1 Model

We use the UVic 2.9 Earth System model of intermediate complexity (Weaver et al., 2001; Keller et al., 2012) in a noLand configuration with a dynamically coupled atmosphere, sea-ice and ocean component (Gent & McWilliams, 1990; Orr et al. 1999; Koeve et al., 2020). A detailed description of this model version is given in the supplementary methods section. The three-dimensional ocean component has a spatial resolution of 3.6° longitude and 1.8° latitude and consists of 19 vertical levels with 50 m thickness close to the surface and up to 500 m in the deep ocean. The used model version contains a fully simulated carbon cycle including dissolved inorganic carbon (DIC) and alkalinity as prognostic tracers, an ecosystem model representation of the biological (soft tissue) carbon pump in which we assume a fixed C-N-P organic matter stoichiometry (Keller et al., 2012), as well as a simple $CaCO_3$ counter pump approximation (Schmittner et al., 2008). In the model primary production is not sensitive to CO_2 and the nutrients nitrate and phosphate are simulated as prognostic tracers, while iron-limitation is prescribed via a concentration mask at the oceans surface layer (Galbraith et al., 2010).

In our UVic 2.9 noLand model version all interactions with the land-component are disabled in order to isolate the effects of AU exclusively on the ocean. This allows us to better understand and distinguish the involved processes and effects of AU especially on the marine carbon cycle.

2.2 Simulating AU

The simulation of AU is adopted from previous studies conducted with an earlier version of the UVic model (Oschlies et al., 2010; Keller et al., 2014). Model tracers like nutrients, temperature, DIC and alike are transferred via AU adiabatically from the lowest grid box at the end of the pipes to the surface grid box at a rate of 1 cm/day averaged over the area of the grid box, while a compensating down-welling flux through all intermediate levels ensures volume conservation. A model algorithm is used at model runtime to automatically deploy the ocean pipes only where (a) the phosphate concentration is lower than a threshold concentration at the sea surface (0.4 $mmol/m^3$ in this study) and (b) complete uptake of upwelled macronutrients would lead to a reduction in local surface-water pCO_2. This procedure ensures that pipes are only deployed in regions where CO_2 outgassing is unlikely (Fig S1a). Additionally, the length of the pipes is limited to 1000 m and optimized by the algorithm to maximize for additional local CO_2 uptake (Fig S1b). Besides nutrients, AU has an impact on all other tracers

including DIC, alkalinity, salinity and temperature. Since our model does not include a dynamic iron cycle, we follow the approach of Keller et al. (2014) and assume that AU relaxes any iron limitation at the sea surface in regions where pipes are deployed. Hence, our experiments considered a best-case scenario for the impact of a close to global application of AU on a Redfield-like biological carbon pump.

2.3 Separation of marine carbon pumps

The separation of the marine carbon pumps is achieved by introducing two idealized tracers to the model, which measure the individual impact on the carbon cycle via the biological carbon pump (DIC^{rem}) and the solubility pump (DIC^{pre}) (Bernardello et al., 2014; Koeve et al., 2020). The idealized tracer DIC^{rem} is set to zero upon any contact with the atmosphere and increases in the interior ocean by the amount of DIC released into the water column via organic matter degradation, thus exclusively counting the amount of DIC tracing back to the biological carbon pump. The idealized tracer DIC^{pre} adopts the value of total DIC at the surface layer and preserves it while being transported to greater depth through ocean circulation. Therefore, DIC^{pre} exclusively counts the amount of DIC added to the interior ocean via physical-chemical processes at the ocean's surface that are associated with the solubility pump. There is no explicit idealized tracer of DIC stored in the interior ocean by means of the $CaCO_3$ counter pump. DIC^{ca}, however, may be diagnosed from $DIC^{ca} = DIC - DIC^{pre} - DIC^{rem}$. As discussed below, any change in DIC^{ca} should not be confused with the impact of a changing $CaCO_3$ counter pump on atmospheric pCO_2. The idealized tracer Ideal-Age (calculated similar compared to DIC^{rem}) counts the time of a water mass since it was last in contact with the atmosphere and therefore, provides additional information about the age of a water mass in the interior ocean (England, 1995; Koeve & Kähler, 2016). All three idealized tracers are influenced by ocean circulation and mixing, but do not interact with other model tracers.

2.4 Experimental Design

Following model spin-up under preindustrial conditions (see Supplementary Methods) we simulate the historical period from the year 1765 to 2006 with CO_2-emissions to the atmosphere, which are consistent with historical fossil fuel and land-use carbon emissions and apply from 2006 to 2100 different CO_2-emission forcings consistent with RCP 2.6, 4.5, 6.0 and 8.5 (Meinshausen et al., 2011), which are corrected for the noLand model configuration (Table 1 and Fig S2) (Koeve et al., 2020). An idealized No-Emission model simulation applies AU in a hypothetical world without any historical or future CO_2

emissions. We simulated the effects of AU in the ArtUp-simulations for the time period 2020 to 2100 and performed respective reference simulations with no simulated AU for comparisons. By comparing the ArtUp- to the Reference-simulation (i.e. ArtUp – REF) conducted under the same CO_2 emission scenario we can explicitly study the effects of applied AU on the ocean. We compared these results with respect to the different CO_2 emission scenarios to study the effectiveness of AU under different CO_2 emission scenarios.

3 Results

3.1 Impact of AU on the Ocean's Carbon Budget

AU leads to a carbon drawdown from the atmosphere into the ocean in comparison to the respective reference simulation (REF), while the additional ocean's carbon uptake is strongly dependent on the RCP CO_2 emission scenario over the course of the experiments (Fig 1a). Under the RCP 8.5 and RCP 6.0 CO_2 emission scenarios, AU leads to an almost linear and continuous carbon drawdown from the atmosphere into the ocean (1.01 Pg C / year for RCP 8.5), while the carbon drawdown under the RCP 4.5 CO_2 emission scenario starts to slow down after 50 years of pipe deployment. Under the RCP 4.5 CO_2 emission scenario the cumulative carbon drawdown after 80 years is already ~50% less compared to the RCP 8.5 CO_2 emission scenario simulation. The RCP 2.6 CO_2 emission scenario and the No-Emission simulation show an even earlier and stronger decline in the ocean's carbon uptake, until they reach a plateau after a few decades (0.32 Pg C / year for RCP 2.6). The dependency of the additional ocean's carbon uptake on the CO_2 emission scenario coincides with an increase in the intensity (cumulative carbon uptake / km^2 pipe area) of AU to draw down carbon from the atmosphere (Fig S3). The model simulations show that the potential of AU to draw down carbon from the atmosphere increases with higher CO_2 emission scenarios, while the carbon drawdown potential decreases and even stagnates under lower CO_2 emission scenarios.

3.2 Biological Carbon Pump vs. Solubility Pump

In the global deployment scenario, the biological carbon pump responds to AU under every CO_2 emission scenario by an additional carbon uptake and only shows a moderate emission scenario dependency, while the solubility pump shows a strong emission scenario dependency and can even release carbon into the atmosphere and thereby counter the biological carbon pump uptake under low

emission scenarios (Fig 1b). Since we apply a fixed C-N-P stoichiometry for primary production and degradation in our model, the additional carbon uptake via the biological carbon pump cannot be explained by pumping up re-mineralized nutrients, but by introducing preformed nutrients from the interior ocean to the sea surface (Fig 2a). Preformed nutrients are nutrients, which leave the surface ocean by circulation in temperate and high latitude waters (without being taken up by primary producers e.g. due to iron or light limitation), while re-mineralized nutrients leave the surface ocean in the form of sinking organic matter. Thus, the degradation of organic matter in the interior ocean releases re-mineralized nutrients as well as its DIC^{rem} equivalent. Preformed nutrients do not have a one to one DIC equivalent, since DIC^{rem} is controlled by the stoichiometry of organic matter degradation, whereas DIC^{pre} is controlled by physical-chemical processes at the ocean's surface (Fig S4). Therefore, preformed nutrients pumped to the sea surface via AU do not come with a CO_2 counterpart and can lead to an additional carbon uptake via the biological carbon pump. The fixed stoichiometry also implies that pumping up DIC^{rem} to the sea surface will not lead to an outgassing of CO_2 into the atmosphere as long as its re-mineralized nutrients get taken up close to the pipes by primary producers again.

The response of the solubility pump can be explained by a combination of several processes including pumping up alkalinity, preformed DIC and changes in water temperature. In the global average, the alkalinity concentration in our model increases with depth due to $CaCO_3$ production at the sea surface and dissolution in the interior ocean (Fig S5a). By simulating AU we pump up alkalinity, on average, from the deep ocean back to the sea surface, which translates into alkalinity enhancement at the sea surface similar to what is intended by artificial ocean alkalinity enhancement by adding minerals like olivine to the ocean surface (Köhler et al., 2010; Hartmann et al., 2013). Artificial enhancement of ocean alkalinity and AU alike leads to a CO_2 flux from the atmosphere into the ocean (Fig 2b) (Keller et al., 2014). Since the amount of alkalinity added to the sea surface is about the same under every emission scenario in our experiments (Fig S5b), we do expect a similar CO_2 uptake effect and therefore, this process can most likely not explain the dependency of the solubility pump to the emission scenario. AU also results in a change in water temperatures, since the water pumped up from the deep ocean is significantly colder compared to the surface water. However, the deeper and colder water pumped up gets heated up at the sea surface, which decreases the CO_2 solubility of the initially colder water mass (Fig 2c). Assuming perfect equilibration with the atmosphere in the water mass formation region, this should results in a carbon flux from the ocean to the atmosphere. At the same time pumping up cold

211 water via AU causes a net decrease of surface water temperatures compared to the reference case
212 without AU (Fig 2d). This causes a relative increase of surface water CO_2 solubility compared to the
213 reference, which results in a carbon flux from the atmosphere into the ocean. Both carbon fluxes related
214 to temperature effects will counteract each other, but since, over the area where pipes are deployed, the
215 relative temperature increase of the pumped up water is much greater than the relative temperature
216 decrease of the surface water (Fig S6), the net effect on the carbon flux is expected to result in CO_2
217 outgassing into the atmosphere. Furthermore, AU pumps up DIC^{pre} from the interior ocean to the sea
218 surface and in contact with the atmosphere (Fig 2e). DIC^{pre} is the amount of carbon taken up by the
219 ocean via physical-chemical processes and its concentration in the interior ocean strongly depends on
220 the pCO_2^{atm} concentration and water temperature at the time and location of the water mass formation
221 region. The water pumped up via AU is mostly old enough to be equilibrated under preindustrial
222 pCO_2^{atm} levels (~275 ppm; Fig 3c). Pumping it up to the sea surface and bringing it in contact with an
223 elevated pCO_2^{atm} level (>400 ppm, except for RCP 0.0) results in a carbon flux from the atmosphere into
224 the ocean, which also increases under higher emission scenarios (Fig S7). While a quantitative
225 separation of the individual processes influencing the response of the solubility pump is challenging
226 (and beyond the scope of this paper), we propose from the discussion above that the outgassing under
227 the RCP 2.6 emission scenario is most likely dominated by the temperature increase of the pumped up
228 water. Under higher emission scenarios the positive impact of pumping up water to the sea surface,
229 which had been equilibrated under preindustrial atmospheric CO_2 levels exceeds the negative impact of
230 the temperature increase of the pumped up water mass.
231
232 3.3 Carbon Storage Depths and Location
233 For the RCP 8.5 emission scenario 56.1 Pg C (69.5 %) of the AU-induced air-sea carbon flux gets added
234 below the maximum pipes source depths of 1200m and can be referred to as stored over the next
235 centuries (Tab. S1) (Lampitt et al., 2008; Siegel et al., 2021). Using pump-specific tracers, we diagnose
236 individual shares of 11.6 Pg C (20.7 %) for the biological carbon pump and 22.6 Pg C (40.2%) for the
237 solubility pump. The remaining 21.9 Pg C (39.1%), computed as residual (see Methods), is assumed to
238 be associated with the carbon export via the $CaCO_3$ counter pump (but see discussion below). Therefore,
239 63.5% of the total carbon taken up via the solubility pump and only 29% of the total carbon taken up via
240 the biological carbon pump gets stored below 1200m. The inefficiency of the biological carbon pump to
241 add carbon below 1200m gets amplified through AU by a reduction in the global transfer efficiency

(T_{eff}) of -7.2% (Tab. S2). The transfer efficiency, here calculated as the integral of remineralized detritus$^{\geq 1200m}$ / remineralized detritus$^{\geq 130m}$, gives an estimate of how strong the organic matter degradation is between the carbon export depth and the carbon storage depth. A reduction in T_{eff} triggered by AU indicates a higher organic matter degradation rate between 130m and 1200m (reasons discussed below). Overall, the budget changes of DIC, DIC^{pre} and DIC^{rem} show that a substantial amount of the carbon added to the ocean via AU gets stored below the maximum source depths of the pipes, with the solubility pump showing a high efficiency in transporting the additional carbon to the deep ocean.

The increased carbon uptake of the ocean via AU below 1200m is unevenly distributed in the ocean with hotspots in the North Atlantic, North Pacific and around the equator (Fig 3b). The solubility pump is the main driver for the additional carbon storage in the North Atlantic (Fig 3d). The additional carbon uptake of the solubility pump has its origin at the atmosphere to ocean boundary and the shallow pipes in the north Atlantic (Fig 3a) cannot explain the carbon transport below the pipes source depth. Thus, we propose that one contributing factor to the high efficiency of the solubility pump in this region is the large-scale ocean circulation. The pipes are long enough to pump up water, which was equilibrated under a lower pCO_2^{atm} level, and thus stimulates the carbon drawdown via the solubility pump (Fig 3e), while the large-scale ocean circulation and deep water formation appears to be responsible for the carbon export below the pipes source depth. The CO_2 uptake via the biological carbon pump below 1200m related to AU is dominated by the central-east Pacific region (Fig 3f). This region has a strong naturally occurring stratification, which gets first undermined by the pipe's pumping action and second weakened by the temperature exchange between the surface water and the deep ocean. Thus, the temperature gradient between the surface water and the deep ocean decreases and allows preformed nutrients to enter the surface ocean more efficiently. This results in an additional carbon uptake via an enhanced biological carbon pump and leads to a greater export of DIC^{rem} below 1200m.

4 Discussion

The residual portion of 21.9 Pg C below 1200 m that is attributed neither to the biological carbon pump nor to the solubility pump, is associated with the $CaCO_3$ counter pump. This additional deep carbon flux leaves the impression of the $CaCO_3$ counter pump being important in terms of additional ocean CO_2

uptake, but, as is well known, the $CaCO_3$ counter pump cannot constitute a CO_2 flux into the ocean due to its flux of alkalinity being twice as high as the DIC flux (Riebesell et al., 2009). In our model, the production of $CaCO_3$ is linked to the detritus production of the ecosystem model (see suppl. Methods) and thus, gets indirectly stimulated via any increase in primary production. However, more intensive $CaCO_3$ export from the surface ocean would reduce the surface ocean CO_2-buffer capacity and reduce CO_2 uptake via the solubility pump. Due to the non-linearity of the CO_2 system it is not straightforward to quantify how the apparent storage (i.e. increase in DIC^{ca}, Fig S8) associated with this increase of the $CaCO_3$ counter pump translates into a CO_2-flux between ocean and atmosphere.

Concerning the reduction of the transfer efficiency under AU, we propose that this might be a result of an increase in water temperature below the cooled surface layer (Fig S9). Organic matter degradation speeds up under higher water temperatures, which results in shallower degradation depth. AU and the compensating downward flow result in a net downward heat flux to greater depth. This side effect of AU was discovered and discussed in previous papers and causes, after AU termination, a strong increase in surface air temperature and pCO_2^{atm} levels beyond the reference simulations (Oschlies et al., 2010; Keller et al., 2014). Here we report that the AU-induced heat transport to greater depth also has a negative impact on the organic matter transfer efficiency during AU deployment.

5 Conclusion and outlook

Our study suggests that the additional carbon uptake of the ocean due to AU is strongly dependent on the CO_2 emission scenario. The biological carbon pump is able to take up additional carbon in the assumed global AU deployment under every emission scenario, but shows a low efficiency in exporting DIC^{rem} below the maximum pipe source depth of 1200m except for the central-east Pacific region. This suggests that most of the CO_2 uptake stimulated by AU and attributable to an increase of the biological carbon pump will potentially be rather short lived. The main driver for the AU-enhanced biological carbon pump is the decreased stratification and the increased access of primary producers to preformed nutrients, while the decrease in the transfer efficiency might be a side effect of faster organic matter degradation due to higher water temperatures below the sea surface.

The solubility pump shows a strong CO_2 emission scenario dependency and can lead to CO_2 outgassing under low emission scenarios, which can almost completely mitigate the additional CO_2 uptake via the biological carbon pump. Under high emission scenarios, the solubility pump can also take up equal amounts of additional CO_2 compared to the biological carbon pump. The solubility pump shows a high efficiency in exporting DIC^{pre} below the maximum pipes source depth and the large-scale ocean circulation in the North Atlantic including deep-water formation seems to play a key role in this regard.

Additional studies including new model experiments might be able to quantify the single processes associated with the solubility pump and to further investigate the high efficiency CO_2 export regions identified in this study. Going beyond the Redfield world and assuming higher C-N ratios in organic matter produced via AU as proposed recently from experimental work (Baumann et al., 2021), as well as simulating the potentially limited supply of iron (Tagliabue et al., 2017) in pipe-covered areas could further impact projections of the quantitative potential of the biological carbon pump in this CDR technique.

Acknowledgement

We acknowledge discussions with colleagues from the Biogeochemical Modelling research unit at GEOMAR. M.J. acknowledges funding from German BMBF, Project Test-ArtUp (Grant Number: 03F0897A). This is a contribution to the CDRmare research mission funded by the German Alliance for Marine Research (DAM).

Data statement

Model output and scripts for data processing are available from data.geomar.de (https://hdl.handle.net/20.500.12085/9e4c269c-8fa3-4bb9-994f-e8c7a5cdefbb)

References

IPCC, 2018: Summary for Policymakers. In: *Global Warming of 1.5°C. An IPCC Special Report on the impacts of global warming of 1.5°C above pre-industrial levels and related global greenhouse gas*

emission pathways, in the context of strengthening the global response to the threat of climate change, sustainable development, and efforts to eradicate poverty [Masson-Delmotte, V., P. Zhai, H.-O. Pörtner, D. Roberts, J. Skea, P.R. Shukla, A. Pirani, W. Moufouma-Okia, C. Péan, R. Pidcock, S. Connors, J.B.R. Matthews, Y. Chen, X. Zhou, M.I. Gomis, E. Lonnoy, T. Maycock, M. Tignor, & T. Waterfield (eds.)]. Cambridge University Press, Cambridge, UK and New York, NY, USA, pp. 3-24, doi:10.1017/9781009157940.001.

Baumann, M., Taucher, J., Paul, A. J., Heinemann, M., Vanharanta, M., Bach, L. T., Spilling, K., Ortiz, J., Aristegui, J., Hernández, N., Baños, I., & Riebesell, U. (2021). Effect of intensity and mode of artificial upwelling on particle flux and carbon export. *Frontiers in Marine Science*, 1579, doi:10.3389/fmars.2021.742142.

Bernardello, R., Marinov, I., Palter, J. B., Galbraith, E. D., & Sarmiento, J. L. (2014). Impact of Weddell Sea deep convection on natural and anthropogenic carbon in a climate model. *Geophysical Research Letters*, *41*(20), 7262-7269, doi:10.1002/2014GRL061313.

Duteil, O., Koeve, W., Oschlies, A., Aumont, O., Bianchi, D., Bopp, L., Galbraith, E., Matear, R., Moore, J. K., Sarmiento, J. L., & Segschneider, J. (2012). Preformed and regenerated phosphate in ocean general circulation models: can right total concentrations be wrong?. *biogeosciences*, *9*(5), 1797-1807, doi:10.5194/bg-9-1797-2012.

Dutreuil, S., Bopp, L., & Tagliabue, A. (2009). Impact of enhanced vertical mixing on marine biogeochemistry: lessons for geo-engineering and natural variability. *Biogeosciences*, *6*(5), 901-912, doi:10.5194/bg-6-901-2009.

England, M. H. (1995). The age of water and ventilation timescales in a global ocean model. *Journal of Physical Oceanography*, *25*(11), 2756-2777, doi: https://doi.org/10.1175/1520-0485(1995)025<2756:TAOWAV>2.0.CO;2.

Galbraith, E. D., Gnanadesikan, A., Dunne, J. P., & His- cock, M. R. (2010). Regional impacts of iron-light colimitation in a global biogeochemical model. *Biogeosciences, 7(3)*, 1043–1064, 2010, doi:10.5194/bg-7-1043-2010.

Gent, P. R., & Mcwilliams, J. C. (1990). Isopycnal mixing in ocean circulation models. *Journal of Physical Oceanography*, *20*(1), 150-155, doi: 10.1146/annurev.fluid.40.111406.102139.

GESAMP (2019). "High level review of a wide range of proposed marine geoengineering techniques," in *Rep. Stud. GESAMP No. 98, (IMO/FAO/UNESCO-IOC/UNIDO/WMO/IAEA/UN/UN Environment/UNDP/ISA Joint Group of Experts on the Scientific Aspect of Marine Environmental Protection)*, eds P.W. Boyd & C.M.G. Vivian (London: International Maritime Organisation), 144.

Hartmann, J., West, A. J., Renforth, P., Köhler, P., De La Rocha, C. L., Wolf-Gladrow, D., Dürr, J., & Scheffran, J. (2013). Enhanced chemical weathering as a geoengineering strategy to reduce atmospheric carbon dioxide, supply nutrients, and mitigate ocean acidification. *Reviews of Geophysics*, *51*(2), 113-149, doi:10.1002/rog.20004.

Keller, D. P., Oschlies, A., & Eby, M. (2012). A new marine ecosystem model for the University of Victoria Earth System Climate Model. *Geoscientific Model Development*, *5*(5), 1195-1220, doi:10.5194/gmd-5-1195-2012.

Keller, D. P., Feng, E. Y., & Oschlies, A. (2014). Potential climate engineering effectiveness and side effects during a high carbon dioxide-emission scenario. *Nature communications*, *5*(1), 1-11, doi:10.1038/ncomms4304.

Koeve, W., & Kähler, P. (2016). Oxygen utilization rate (OUR) underestimates ocean respiration: A model study. *Global Biogeochemical Cycles*, *30*(8), 1166-1182, doi:10.1002/2015GB005354.

Koeve, W., Kähler, P., & Oschlies, A. (2020). Does Export Production Measure Transient Changes of the Biological Carbon Pump's Feedback to the Atmosphere Under Global Warming?. *Geophysical Research Letters*, *47*(22), doi:10.1029/2020GL089928.

Köhler, P., Hartmann, J., & Wolf-Gladrow, D. A. (2010). Geoengineering potential of artificially enhanced silicate weathering of olivine. *Proceedings of the National Academy of Sciences*, *107*(47), 20228-20233, doi:10.1073/pnas.1000545107.

Lampitt, R. S., Achterberg, E. P., Anderson, T. R., Hughes, J. A., Iglesias-Rodriguez, M. D., Kelly-Gerreyn, B. A., Lucas, M., Popova, E. E., Sanders, R., Shepherd, J. G., Smythe-Wright, D., & Yool, A. (2008). Ocean fertilization: a potential means of geoengineering?. *Philosophical Transactions of the Royal Society A: Mathematical, Physical and Engineering Sciences*, *366*(1882), 3919-3945, ISBN:9780521198035.

Lovelock, J. E., & Rapley, C. G. (2007). Ocean pipes could help the Earth to cure itself. *Nature*, *449*(7161), 403-403, doi:10.1038/449403a.

Meinshausen, M., Smith, S. J., Calvin, K. V., Daniel, J. S., Kainuma, M. L. T., Lamarque, J.-F., Matsumoto, K., Montzka, S. A., Raper, S. C. B., Riahi, K., Thomson, A. M., Velders, G. J. M., & van Vuuren, D. (2011). "The RCP Greenhouse Gas Concentrations and their Extension from 1765 to 2300." Climatic Change (Special Issue), DOI:10.1007/s10584-011-0156-z.

Orr, J. C., R. Najjar, C. L. Sabine, & F. Joos (1999), Abiotic-HOWTO, internal OCMIP report, LSCE/CEA Saclay, 25 pp., Gif-sur-Yvette, France.

Oschlies, A., Pahlow, M., Yool, A., & Matear, R. J. (2010). Climate engineering by artificial ocean upwelling: Channelling the sorcerer's apprentice. *Geophysical Research Letters*, *37*(4), doi:10.1029/2009GL041961.

Riebesell, U., Körtzinger, A., & Oschlies, A. (2009). Sensitivities of marine carbon fluxes to ocean change. *Proceedings of the National Academy of Sciences*, *106*(49), 20602-20609, doi:10.1073pnas.0813291106.

Schmittner, A., Oschlies, A., Matthews, H. D., & Galbraith, E. D. (2008). Future changes in climate, ocean circulation, ecosystems, and biogeochemical cycling simulated for a business-as-usual CO2 emission scenario until year 4000 AD. *Global biogeochemical cycles*, *22*(1), doi:10.1029/2007GB002953.

Siegel, D. A., DeVries, T., Doney, S. C., & Bell, T. (2021). Assessing the sequestration time scales of some ocean-based carbon dioxide reduction strategies. *Environmental Research Letters*, *16*(10), 104003, doi:10.1088/1748-9326/ac0be0.

Tagliabue, A., Bowie, A. R., Boyd, P. W., Buck, K. N., Johnson, K. S., & Saito, M. A. (2017). The integral role of iron in ocean biogeochemistry. *Nature*, *543*(7643), 51-59, doi:10.1038/nature21058.

Thoni, T., Beck, S., Borchers, M., Förster, J., Görl, K., Hahn, A., Mengis, N., Stevenson, A., & Thrän, D. (2020). Deployment of negative emissions technologies at the national level: a need for holistic feasibility assessments. *Frontiers in Climate*, *2*, 590305, doi:10.3389/fclim.2020.590305.

Volk, T., & Hoffert, M. I. (1985). Ocean carbon pumps: Analysis of relative strengths and efficiencies in ocean-driven atmospheric CO2 changes. *The carbon cycle and atmospheric CO2: natural variations Archean to present*, *32*, 99-110, doi:10.1029/GM032p0099.

Weaver, A. J., Eby, M., Wiebe, E. C., Bitz, C. M., Duffy, P. B., Ewen, T. L., Fanning, A. F., Holland, M. M., MacFadyen, A., Matthews, H. D., Meissner, K. J., Saenko, O., Schmittner, A., Wang, H., & Yoshimori, M. (2001). The UVic Earth System Climate Model: Model description, climatology, and applications to past, present and future climates. *Atmosphere-Ocean*, *39*(4), 361-428, doi:10.1080/07055900.2001.9649686.

Yool, A., Shepherd, J. G., Bryden, H. L., & Oschlies, A. (2009). Low efficiency of nutrient translocation for enhancing oceanic uptake of carbon dioxide. *Journal of Geophysical Research: Oceans*, *114*(C8), doi:10.1029/2008JC004792.

455 **Tables**

456 **Table 1.** Model simulations experiments conducted with the UVic 2.9 ESM noLand model version.

457 Name	Emission Forcing	Pipe Simulation
458 REF_0.0	No-Emission	No Pipes
459 REF_2.6	RCP 2.6	No Pipes
460 REF_4.5	RCP 4.5	No Pipes
461 REF_6.0	RCP 6.0	No Pipes
462 REF_8.5	RCP 8.5	No Pipes
463 ArtUp_0.0	No-Emission	Pipes
464 ArtUp_2.6	RCP 2.6	Pipes
465 ArtUp_4.5	RCP 4.5	Pipes
466 ArtUp_6.0	RCP 6.0	Pipes
467 ArtUp_8.5	RCP 8.5	Pipes

468

469

470 **Figure Captions**

471 **Figure 1.** Global CO_2 uptake from AU. (a) Time history of cumulative net increase in the ocean's
472 carbon budget via AU compared to respective reference simulation for different CO_2 emission scenarios
473 (ArtUp – REF; Pg C). (b) Cumulative net increase in the ocean's carbon budget in the year 2100 after 80
474 years of pipe deployment (Pg C) divided into the individual carbon uptake of the biological carbon
475 pump (green) and the solubility pump (red).

476

477 **Figure 2.** Theoretical concept of the processes stimulated by AU and their impact on the air-sea CO_2
478 flux. Arrows in the atmosphere indicate air-sea CO_2 flux direction and arrows in the ocean indicate
479 water movement with colors red and blue indicating water temperature increase / decrease. (a) covers
480 the impact of the biological carbon pump, (b) to (e) cover individual processes associated with the
481 solubility pump.

482

483 **Figure 3.** Regional effects of AU for experiments under the RCP 8.5 emission scenarios. (a) Pipe
484 distribution and pipe source depth (m). (c) Average age (since last contact with the atmosphere) of water
485 at pipes source depth (years). (e) CO_2 flux at ocean-atmosphere boundary (positive downward; mol C

486 m^{-2} $year^{-1}$). (b, d, f) Cumulative net change in DIC (b), DIC^{pre} (d) and DIC^{rem} (f) below 1200m depths by
487 the year 2100 compared to the respective reference simulation (ArtUp – REF; Pg C).
488
489
490

FIG_1

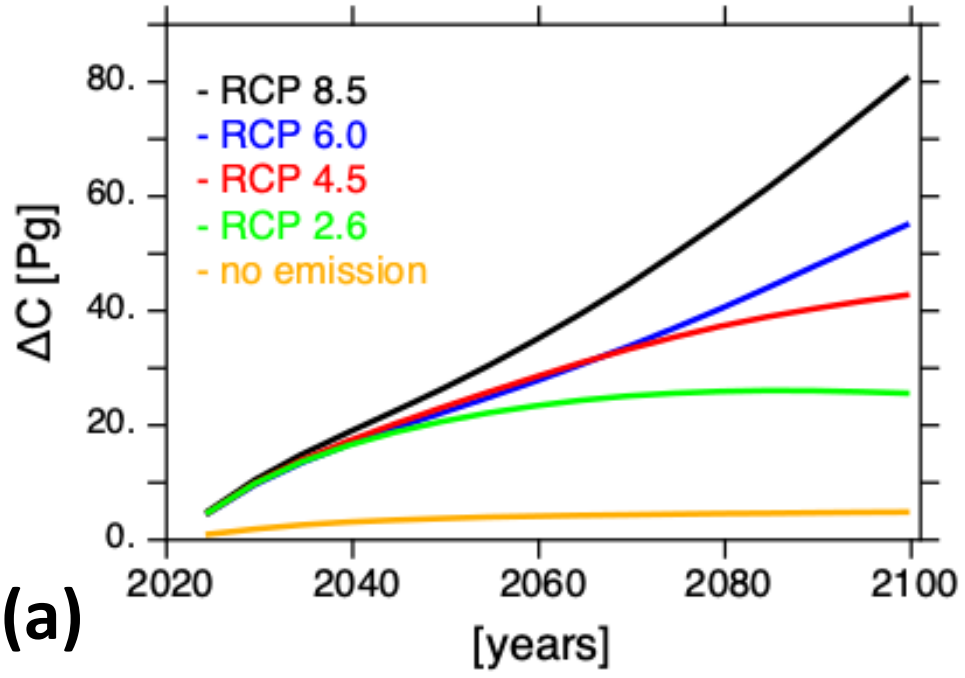
- RCP 8.5
- RCP 6.0
- RCP 4.5
- RCP 2.6
- no emission
ΔC [Pg]
80.
60.
40.
20.
0.
2020
2040
2060
2080
2100
[years]

(a)

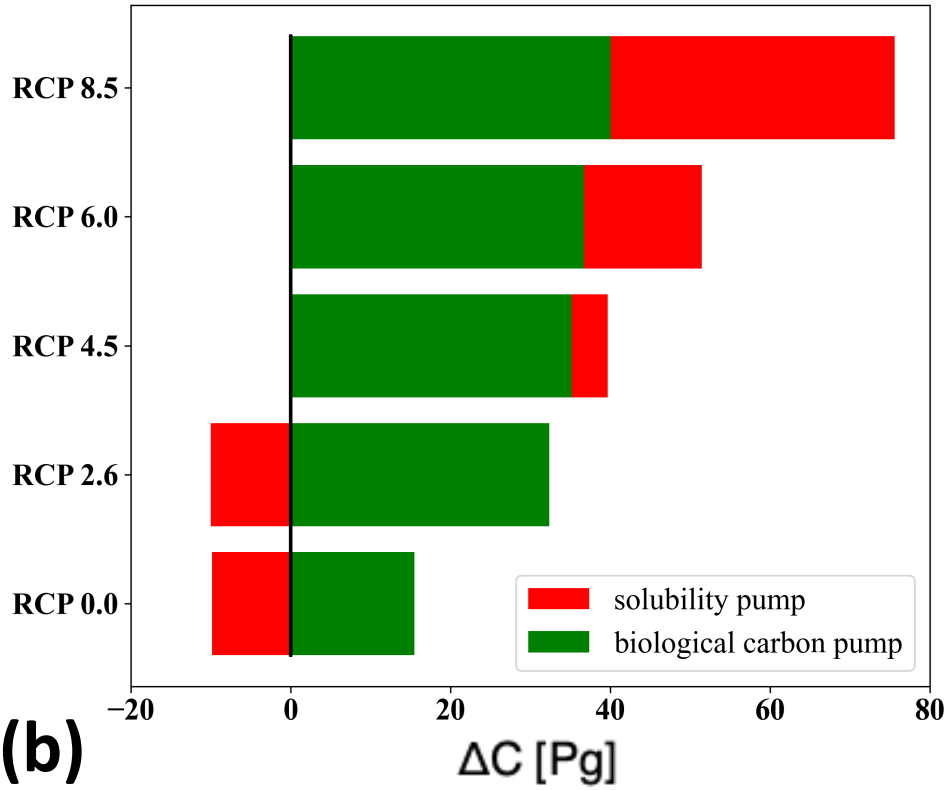
RCP 8.5
RCP 6.0
RCP 4.5
RCP 2.6
RCP 0.0
solubility pump
biological carbon pump
−20
0
20
40
60
80
ΔC [Pg]

(b)

FIG_2

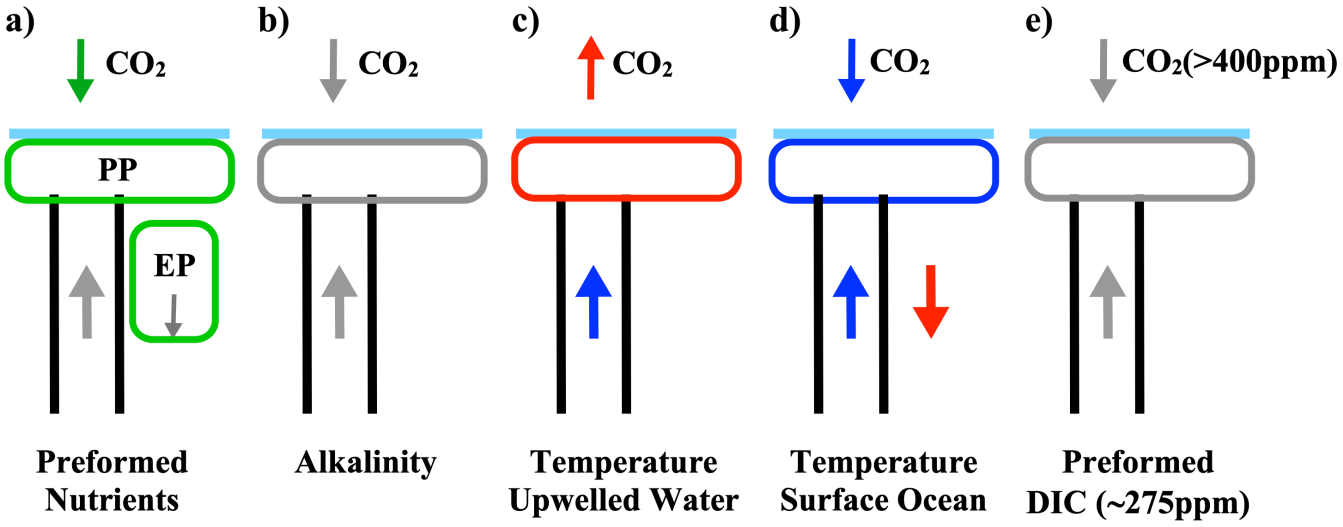
a)
CO2
PP
EP
Preformed Nutrients
b)
CO2
Alkalinity
c)
CO2
Temperature Upwelled Water
d)
CO2
Temperature Surface Ocean
e)
CO2(>400ppm)
Preformed DIC (~275ppm)

FIG_3

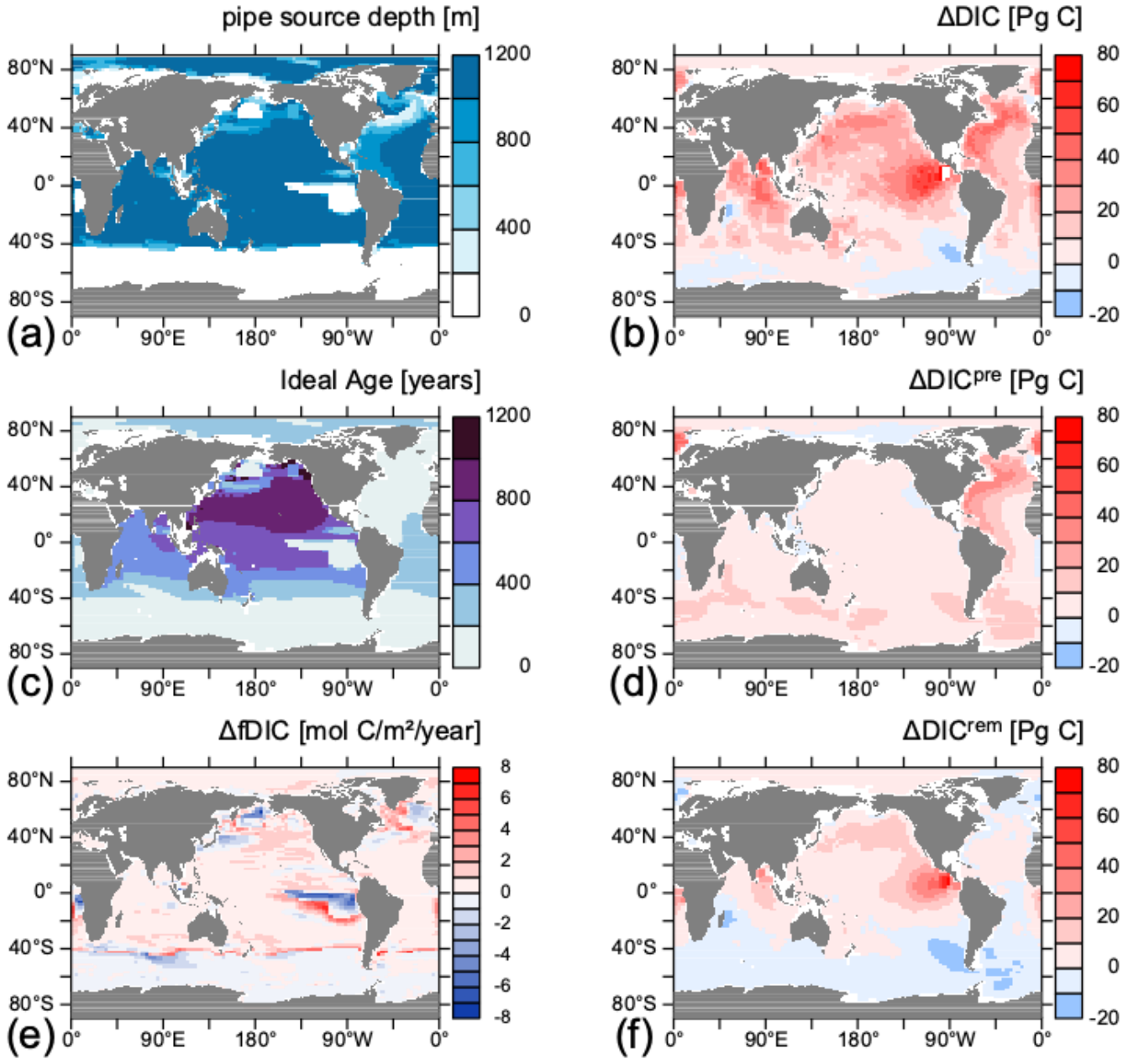
pipe source depth [m]
1200
800
400
0
(a)
ΔDIC [Pg C]
80
60
40
20
0
-20
(b)
Ideal Age [years]
1200
800
400
0
(c)
ΔDIC^pre [Pg C]
80
60
40
20
0
-20
(d)
ΔfDIC [mol C/m²/year]
8
6
4
2
0
-2
-4
-6
-8
(e)
ΔDIC^rem [Pg C]
80
60
40
20
0
-20
(f)
80°N
40°N
0°
40°S
80°S
0°
90°E
180°
90°W
0°

Geophysical Research Letters

Supporting Information for

Artificial Upwelling – A New Narrative

Jürchott, M.[1], Oschlies, A.[1], Koeve, W.[1]

[1]GEOMAR Helmholtz Centre for Ocean Research Kiel, Germany

Contents of this file

Text S1
Table S1 to S2
Figures S1 to S9

Introduction

Here we provide Supplementary Methods (Text S1), Supplementary Tables (S1 to S2) and Supplementary Figures (S1 to S9), which present details of our model experiments.

Text S1.

Supplementary Methods

UVic model

Model experiments are carried out with an ocean-sea-ice-atmosphere version of the UVic Earth System Model Version 2.9 (UVic-2.9.WK2021.noLand) as described in Koeve et al. (2020). UVic (Weaver et al., 2001) is an Earth system model of intermediate complexity (EMIC). Horizontal resolution is 3.6° in longitude and 1.8° in latitude direction. The ocean circulation model (MOM, Modular Ocean Model 2) includes physical parameterizations for diffusive mixing along and across isopycnals and eddy induced tracer advection (Gent & McWilliams, 1990). It has 19 vertical layers and layer thickness increases from 50 m at the surface to 500m in the deep ocean. Wind forcing is prescribed with monthly mean winds from NCAR/NCEP climatological data. The ocean biogeochemistry of this model is described in Keller et al. (2012). In short, the model simulates the nutrients phosphate and nitrate, two groups of phytoplankton (diazotrophs and ordinary phytoplankton), zooplankton, particulate detritus with explicit sinking, oxygen, total dissolved inorganic carbon (DIC) and alkalinity (ALK) as prognostic tracers. Production and degradation of organic matter affect nutrients, oxygen, DIC and ALK with a fixed elemental stoichiometry. Gas exchange of oxygen and DIC is simulated as in Orr et al. (1999). A diagnostic $CaCO_3$ cycle further shapes the distribution of DIC and ALK (Schmittner et al., 2008). The model includes a simple parameterization of iron limitation based on an iron concentration mask adopted from the BLING model (Galbraith et al., 2010). In order to avoid excessively long model spin-up times our idealized model experiments do not simulate sediment processes. Any organic detritus or $CaCO_3$ reaching the bottom of the model is dissolved in the deepest wet box instantaneously.

UVic-2.9.WK2021 includes a number of idealized model tracers, which allow us to measure the individual impact on the carbon cycle via the biological (soft tissue) carbon pump (DIC^{rem}) and the solubility pump (DIC^{pre}) (Bernardello et al., 2014; Koeve et al.,

2020). This model version includes a suite of preformed tracers (preformed phosphate, PO_4^{pre}; preformed oxygen, O_2^{pre}; preformed DIC, DIC^{pre}; preformed alkalinity, ALK^{pre}). In the surface ocean (k=1) preformed tracers are set at every time step to the value of the respective bulk tracer (e.g.PO_4^{pre} == PO_4). In the interior ocean preformed tracers behave like a passive tracer, i.e. they do not have biogeochemical sinks or sources, while being transported and mixed by the ocean's circulation. DIC^{pre} is the preformed tracer of particular interest in this study as it allows us to quantify any changes in solubility pump carbon (see below). For the bulk tracers PO_4, O_2, DIC, ALK, we further simulate several tracers, which accumulate biogeochemical sinks and sources, but are set to zero in the surface ocean (k=1). DIC^{rem} is the respective tracer for the carbon uptake via the biological carbon pump. DIC^{rem} accumulates the sinks and source of organic matter degradation and production below the surface layer (k=1). The tracer behaves similar to the true oxygen utilization tracer (TOU-tracer) employed in Koeve et al. (2020). The idealized tracer Ideal-Age counts the time of a water mass below the surface layer (k=1), since it was last in contact with the atmosphere and therefore, provides additional information about the age of a water mass in the interior ocean (England, 1995; Koeve & Kähler, 2016). All previous mentioned tracers (except Ideal-Age) have the unit of mol m^{-3} in the model output.

Simulation of artificial upwelling

The simulation of artificial upwelling is adopted from previous studies conducted with an earlier version of the UVic model (Oschlies et al., 2010; Keller et al., 2014). Model tracers like nutrients, temperature, DIC and alike are transferred adiabatically from the lowest grid box at the end of the pipes to the surface grid box to simulate the effects of artificial upwelling on the ocean and atmosphere. The length of artificial upwelling pipes does not exceed 1000m and the velocity of upwelled water from the source depth to the surface layer is assumed to be 1cm/day averaged over the area of the grid box. A compensating down-welling flux through all intermediate levels ensures volume conservation. All prognostic tracers, which could have an impact on the stratification or the carbon cycle in the model are pumped up via artificial upwelling (e.g. temperature,

DIC, ALK, PO_4, NO_3, O_2). Since our model does not include a dynamic iron cycle, we follow the approach of Keller et al. (2014) and assume that artificial upwelling relaxes any iron limitation at the ocean surface (k=1) in regions where pipes are deployed (other primary production limiting factors such as light limitation are not affected by artificial upwelling and can limit nutrient uptake). This may be an overly optimistic assumption, since iron concentrations in the ocean interior are under control of scavenging by organic and inorganic particles causing elevated nutrient to dissolved iron ratios in the ocean interior (Tagliabue et al., 2017). Hence, our experiments considered a best-case scenario for the impact of artificial upwelling on a Redfield-like biological pump with constant element ratios (in particular $r_{C:P} = 106$).

The locations in which pipes are switched on and the source length of the pipes are decided at every time step by an algorithm, which is designed to maximize additional carbon uptake of the ocean and takes several initial conditions into account. First, pipes are not switched on in regions with a PO_4 surface water concentration greater than 0.4 mmol m^{-3} assuming that these regions are not limited by macronutrients and adding more nutrients from greater depth to the surface would not result in an enhancement of the biological carbon pump. Second, pipes are not switched on in regions and at depths, where a short term outgassing of CO_2 into the atmosphere is projected. This projection is based on the vertical distribution of tracers and the current pCO_2^{atm} (no horizontal water mass mixing or circulation taken into account by the runtime algorithm). For each of the potential source depth levels (k=2 to k=8), a potential seawater $pCO_2(k)$ is computed from T(k), S(k), ALK(k) and DIC(k) – (PO_4(k) - PO_4(1))*$r_{C:P}$ assuming surface pressure. This assumes complete utilization of upwelled nutrients (e.g. no iron or light limitation). The algorithm selects the k-level (hence pipe length) for which a maximum difference between the current surface pCO_2 and the potential $pCO_2(k)$ is found, i.e. which offers the maximum potential carbon drawdown into the ocean. If this difference is negative, pipes are turned off. Changes over time in the pipe covered area and the global average pipe length are shown in Fig S1.

We note that the 'projected' pCO_2-difference is not necessarily identical with the surface pCO_2 difference between the artificial upwelling experiment and its respective reference run, in particular since the algorithm does not know about the surface pCO_2 in the independent reference experiment (see next section for details). Despite this limitation, regions with pipes turned on but negative (into the atmosphere) CO_2-flux anomaly (Pipe – Reference) are, however, rare and generally restricted to regions with strong horizontal currents (e.g. North Atlantic current, Kuroshio current), compare Fig. 3a and Fig. 3e.

Experiments carried out

Model experiments presented here are based on a spin-up procedure and model evaluation described in detail in Koeve et al. (2020) (see their Supplementary Methods). A reference simulation (without artificial upwelling, REF) is carried out starting in year 1765 and run with historical CO_2 emissions forcing until year 2005 and continued with four emission forcing pathways consistent with RCP 2.6 to RCP 8.5 pCO_2^{atm} concentration forcing (Fig S2) (Meinshausen et al., 2011). For runs with the UVic-2.9.WK2021.noLand model, emissions have been corrected for land-atmosphere interactions (see Koeve et al., 2020 for details). In this idealized model study we do not consider the impact of non-CO_2 climate forcing (e.g. from N_2O, CH_4, aerosols) in particular since the UVic model lacks a prognostic atmospheric chemistry model and hence respective sinks of e.g. N_2O and CH_4 would not be well defined. The CO_2 emissions applied, represent CO_2 from fossil fuel burning and from land-use changes, in particular deforestation. A fifth simulation (No Emissions) applying no CO_2-emissions is started from the year 1765 model state and run for 335 years. Simulations of artificial upwelling start in year 2020 and last until year 2100. We present results for this period only.

Separating the effects of artificial upwelling on marine carbon pumps

We use idealized tracers in order to evaluate how marine carbon storage is modified by artificial upwelling. In principle following concepts described in e.g. Bernardello et al.

(2014) we separate carbon storage associated with three marine carbon pumps (Volk & Hoffert, 1985) as follows.

Biological carbon pump: While pumping nutrients to the surface has the potential to increase net primary production and export production of organic matter (Dutreuil et al., 2009; Yool et al., 2009; Oschlies, et al. 2010; Keller et al. 2014), this does not imply that the carbon storage associated with the biological carbon pump increase in lockstep (Koeve et al., 2020). Carbon storage from the biological carbon pump may be quantified from the apparent oxygen utilization or idealized tracers of it (Koeve & Kähler, 2016; Koeve et al., 2020) and the oxygen demand of organic matter degradation. Here we employ an explicit idealized DIC^{rem} tracer (Bernardello et al., 2014). This tracer is set to zero in the surface ocean (k=1) at every time step and accumulates the carbon from organic matter degradation and formation in all other model layers (the interior ocean). Note that this tracer is not affected by $CaCO_3$ production or dissolution.

Solubility pump: DIC^{pre} is used in this study in order to quantify the uptake of CO_2 of the ocean via physical-chemical processes (Bernardello et al., 2014; Koeve et al., 2020). Since we apply different CO_2-emission scenarios in this study and a higher pCO_2^{atm} may increase the ocean's CO_2 uptake via physical-chemical processes (Fig S7a), we can use DIC^{pre} to measure the impact of different emission scenarios in the context of artificial upwelling on the oceans carbon budget and distinguish it from e.g. biological related processes. DIC^{pre} adopts the value of DIC at the surface ocean (k=1) at every time step and preserves it while being transported to greater depth through ocean circulation. Thus, DIC^{pre} exclusively accumulates the CO_2 uptake at the ocean's surface and is influenced by e.g. pCO_2^{atm} (emission scenario), water temperature changes or other carbon-climate feedbacks.

$CaCO_3$ counter pump: The used UVic version contains a simple $CaCO_3$ counter pump approximation, but there is no explicit tracer of DIC stored in the interior ocean by means of the $CaCO_3$ counter pump. DIC^{ca}, however can be computed from $DIC^{ca} = DIC - DIC^{pre} - DIC^{rem}$. In UVic, the production of $CaCO_3$ (mol C m^{-3} s^{-1}) is connected to the

detritus term of the NPZD (Nutrients - Primary Producers - Zooplankton - Detritus) ecosystem model and equivalent to 0.03 times the detritus production (same unit), while after production being immediately distributed and dissolved over depth following a declining exponential function (Schmittner et al., 2008). This process results in an export of DIC^{ca} and a respective twice as large ALK export from the surface to the interior ocean (see main text Discussion). Due to this well-known aspect of the $CaCO_3$ counter pump any increase (decrease) of it will constitute a loss (gain) of CO_2 of the ocean. Hence the explanatory power of a DICca tracer, which would indicate the opposite, is quite limited.

Tables

Table S1. Changes in global DIC budget and below 1200m in Pg C between the experiments ArtUp_8.5 and REF_8.5 accumulated by the year 2100.

	DIC	DIC^{pre}	DIC^{rem}	DIC^{ca}
ΔDIC (Pg C)	80.61	35.53	40.05	5.03
$\Delta DIC^{\geq 1200m}$ (Pg C)	56.06	22.55	11.61	21.90

Table S2. Remineralized detritus in Pg C / year integrated below 130m and below 1200m for the experiments ArtUp_8.5 and REF_8.5 for the year 2100, as well as the calculated transfer efficiency.

	rem._detr.$^{\geq 130m}$ (Pg C)	rem._detr.$^{\geq 1200m}$ (Pg C)	T_{eff}
REF_8.5	6.136	0.729	0.119
ArtUp_8.5	10.485	1.168	0.111
Δ	4.349	0.439	-0.008

206

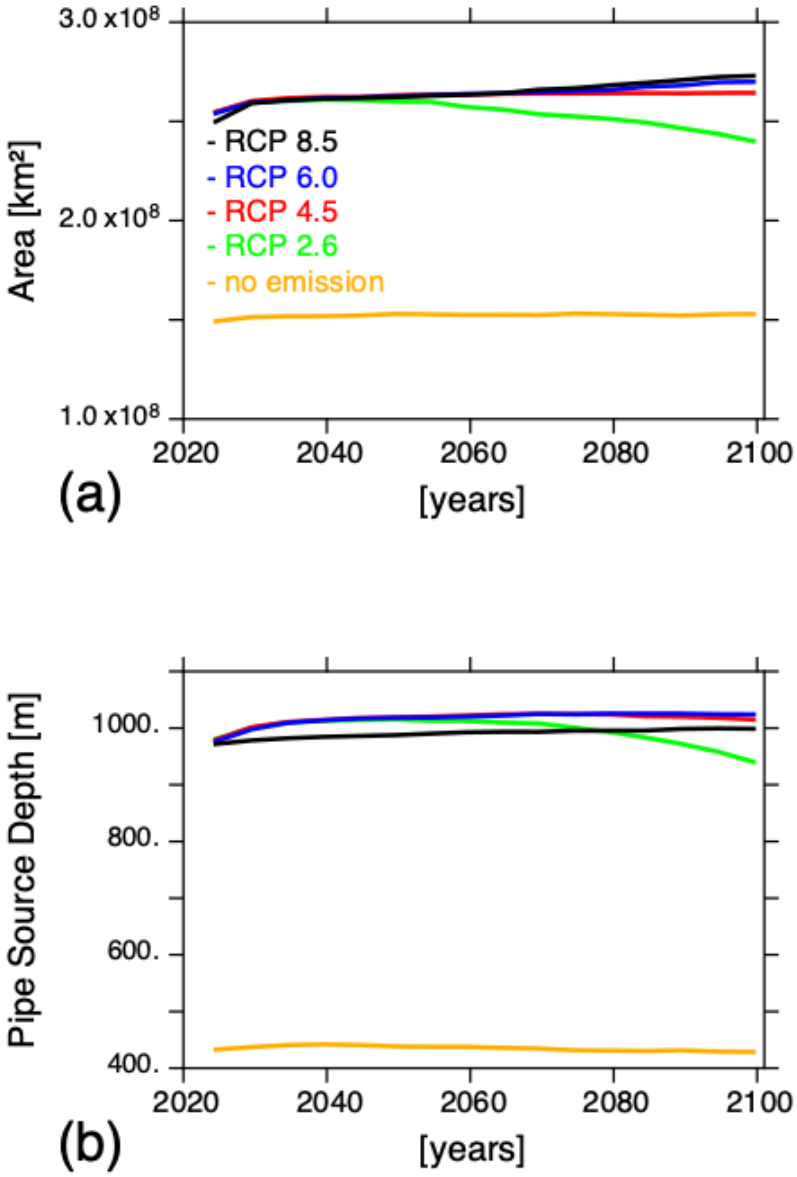

207

208 **Figure S1.** Transient evolution of (a) pipe covered area (km^2) and (b) average pipe

209 source depth for all CO_2 emission scenarios in the ArtUp experiments.

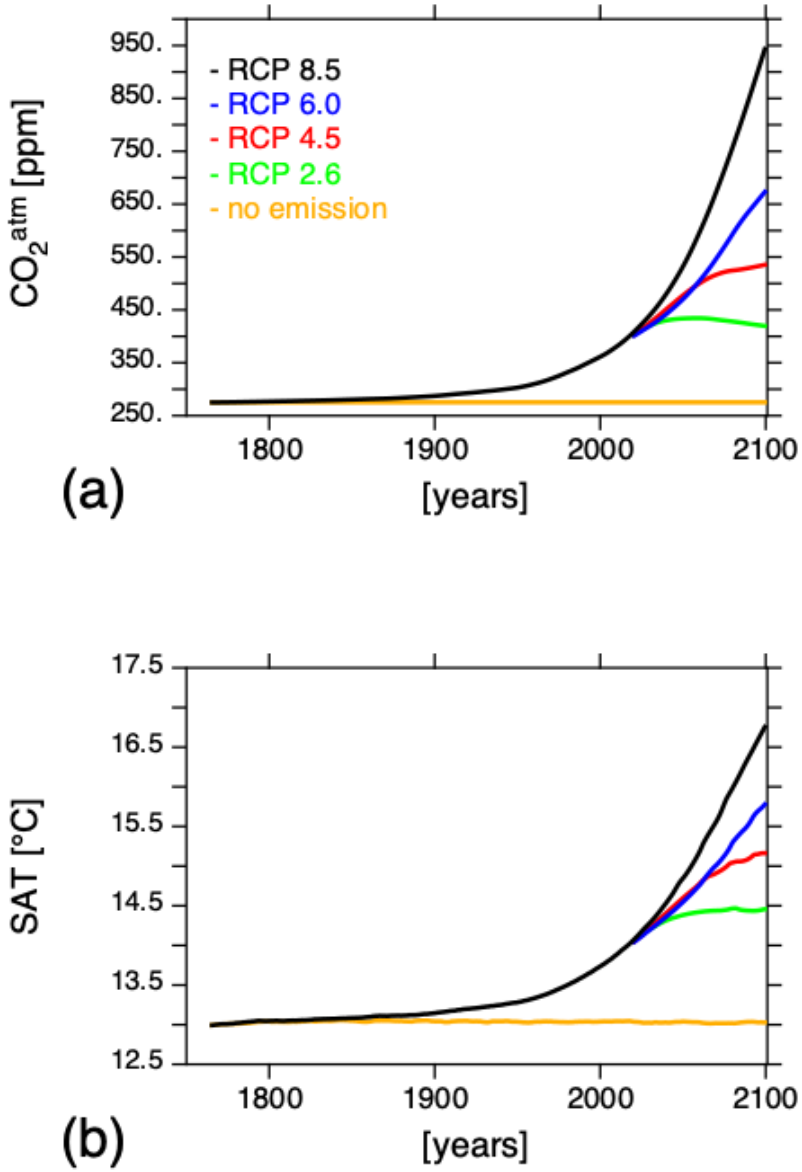

Figure S2. Transient atmospheric properties between the year 1765 and 2100 of (a) pCO_2^{atm} (ppm) and (b) surface air temperature (°C) for all CO_2 emission scenarios in the REF experiments.

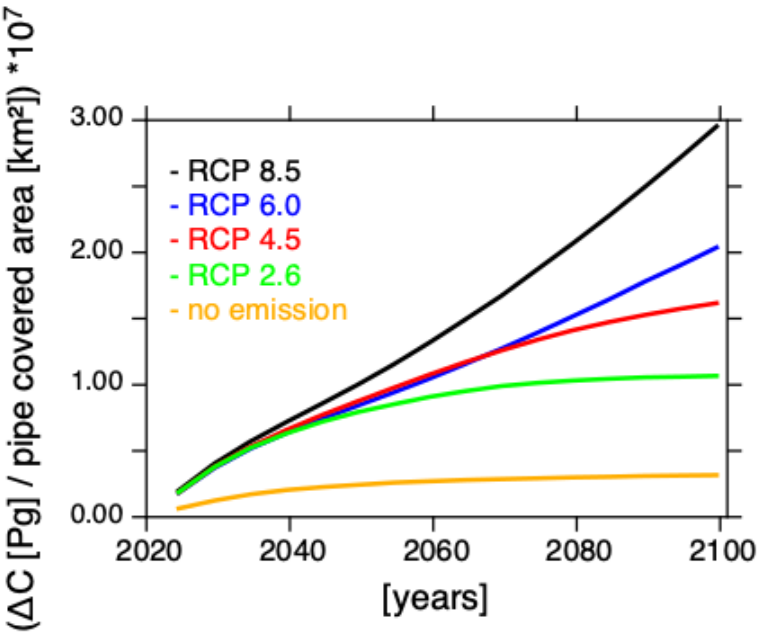

Figure S3. Cumulative changes of the carbon drawdown intensity in the pipe covered area (ΔC Pg per km^2) over time (2020 – 2100) for all CO_2 emission scenarios.

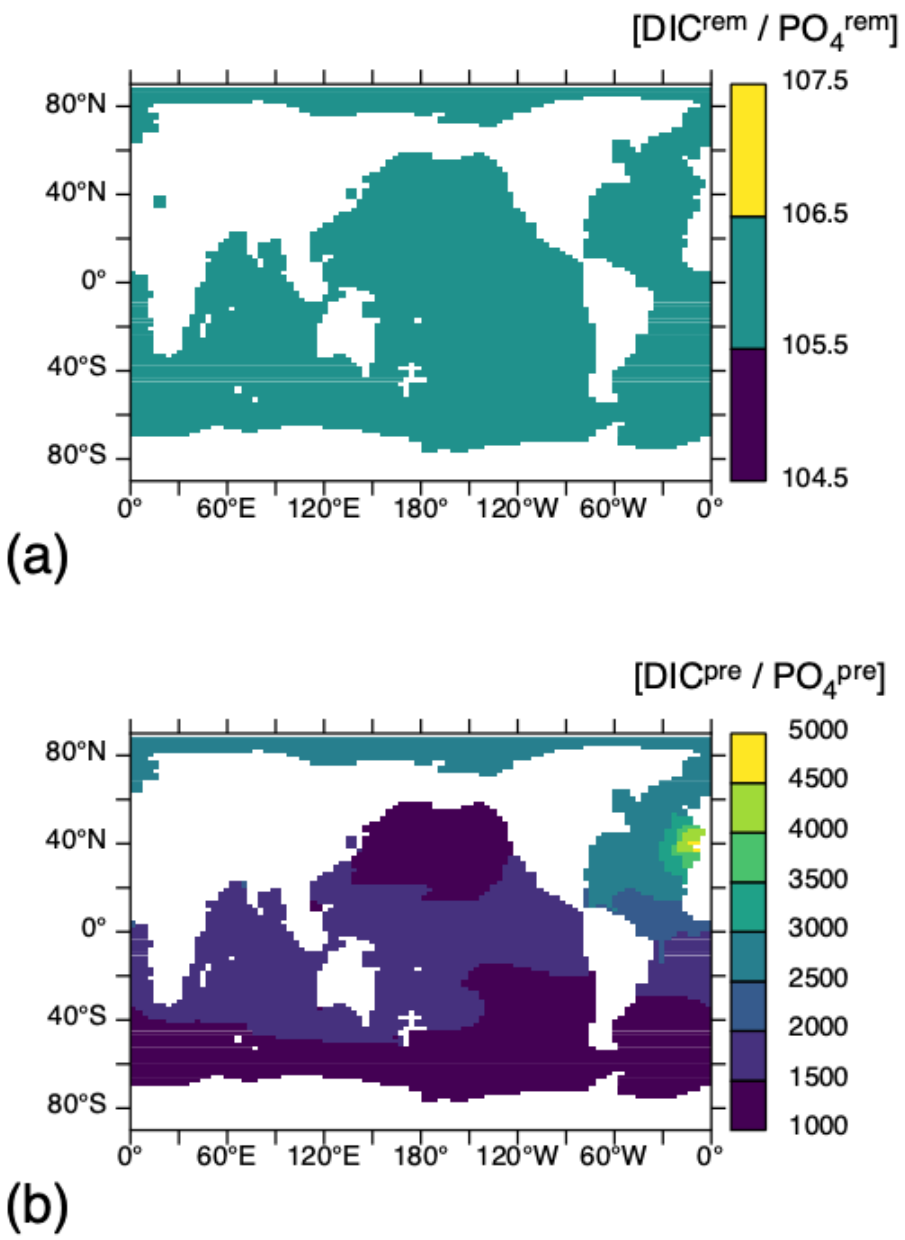

Figure S4. DIC to PO_4 ratio for (a) re-mineralized model tracers and (b) preformed model tracers at 1000 m depth for the REF_8.5 experiment in the year 2100.

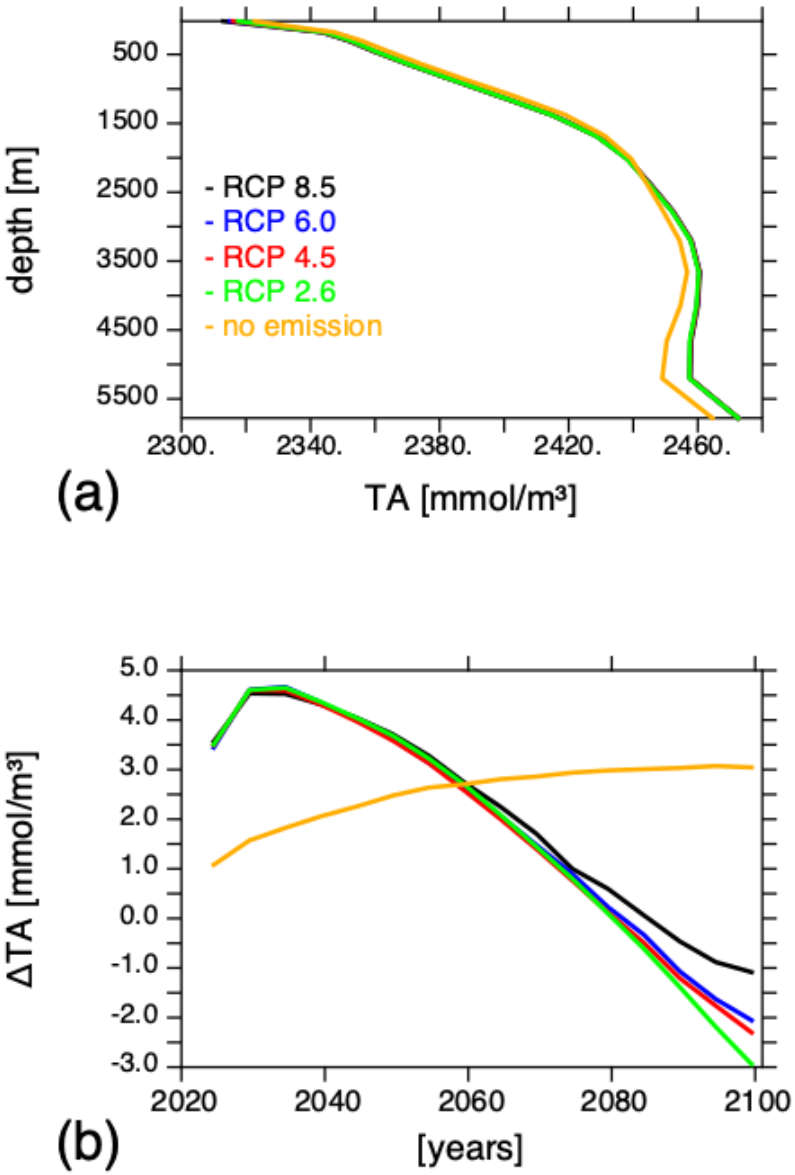

Figure S5. Alkalinity concentrations and changes in the ocean. (a) Globally averaged alkalinity (mmol / m^3) over depth for REF experiments in the year 2100 and (b) changes over time (2020 – 2100) of the alkalinity concentration at the ocean surface (k=1) via artificial upwelling (ArtUp – Ref; mmol / m^3) for all CO_2 emission scenarios. The decrease of surface alkalinity over time under RCP 8.5 to RCP 2.6 is a consequence of the enhanced alkalinity export via the stimulated $CaCO_3$ counter pump (see main text for details).

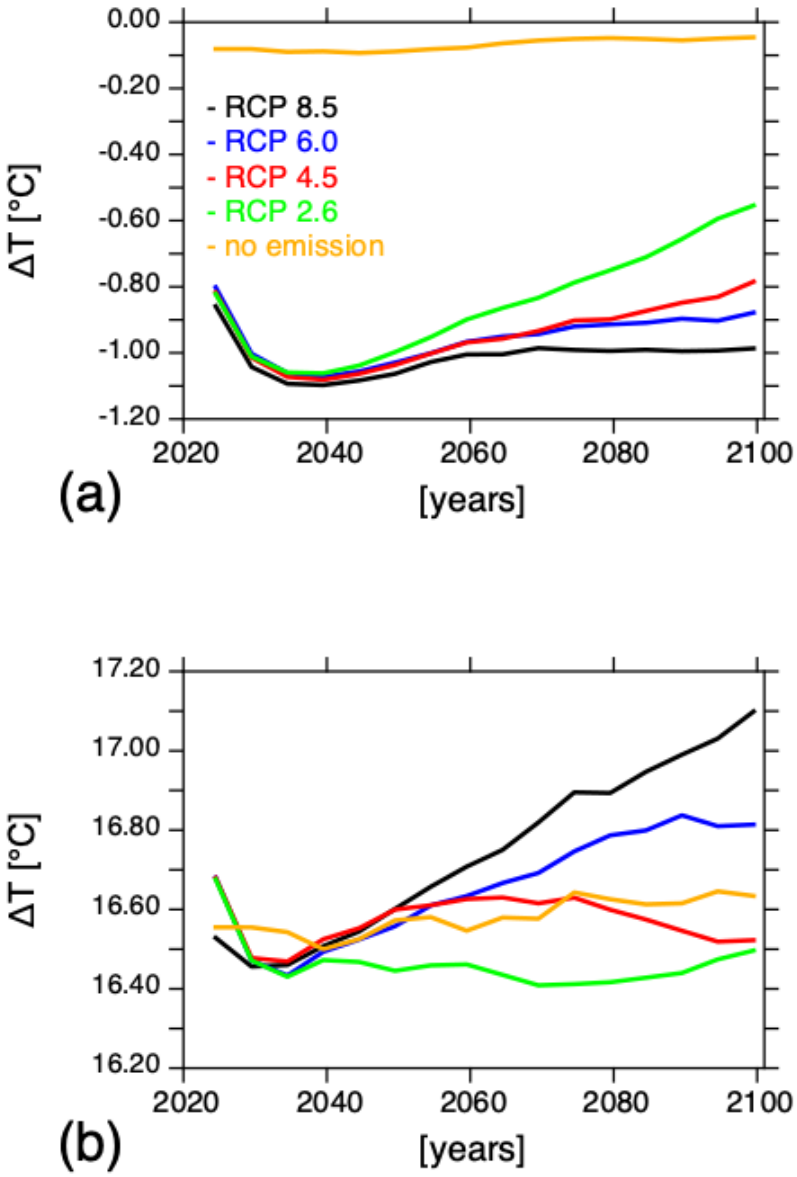

Figure S6. Transient temperature changes in the ocean via artificial upwelling from 2020 to 2100. (a) Global average surface ocean (k=1) temperature change (°C) at pipe location (ArtUp – Ref) and (b) temperature change (°C) of upwelled water at pipe location ($ArtUp^{surface\ ocean} - ArtUp^{pipe\ source\ depth}$).

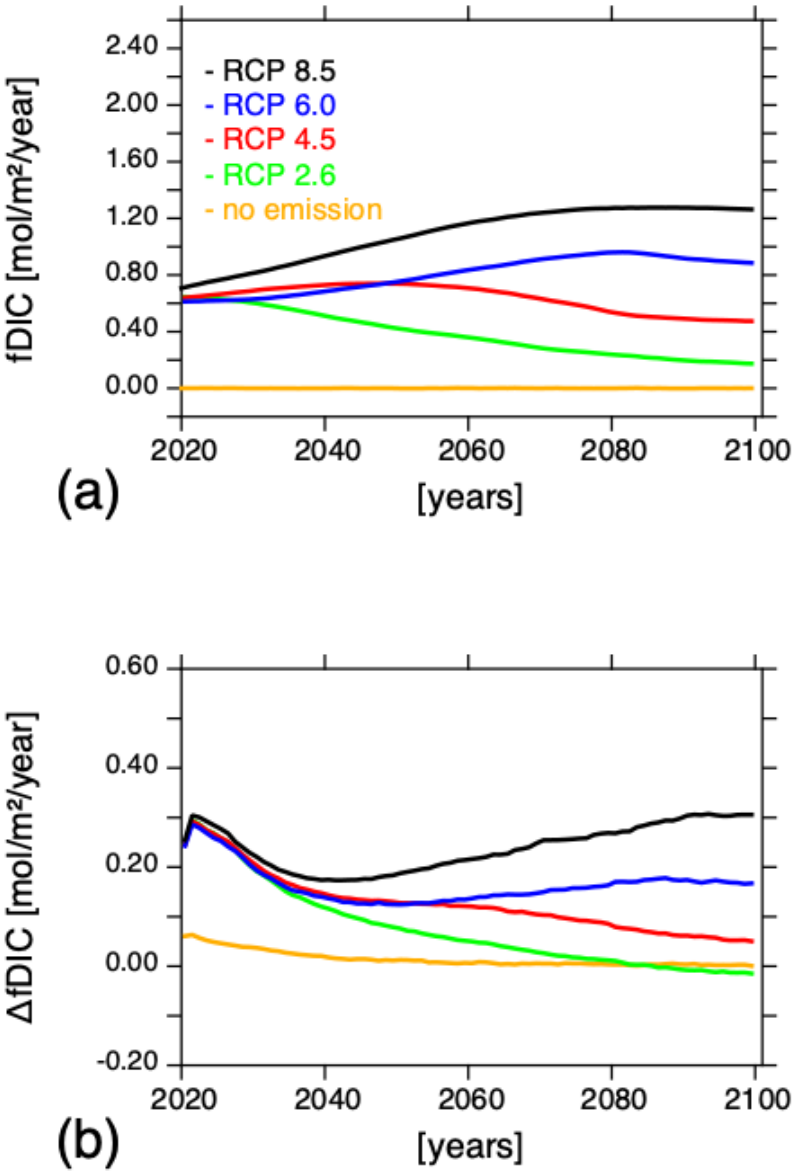

Figure S7. Transient global average CO_2 flux (fDIC) from atmosphere to ocean (mol C / m^2 / $year^1$) from 2020 to 2100 for all CO_2 emission scenarios for (a) REF experiments and (b) changes via artificial upwelling (ArtUp – Ref).

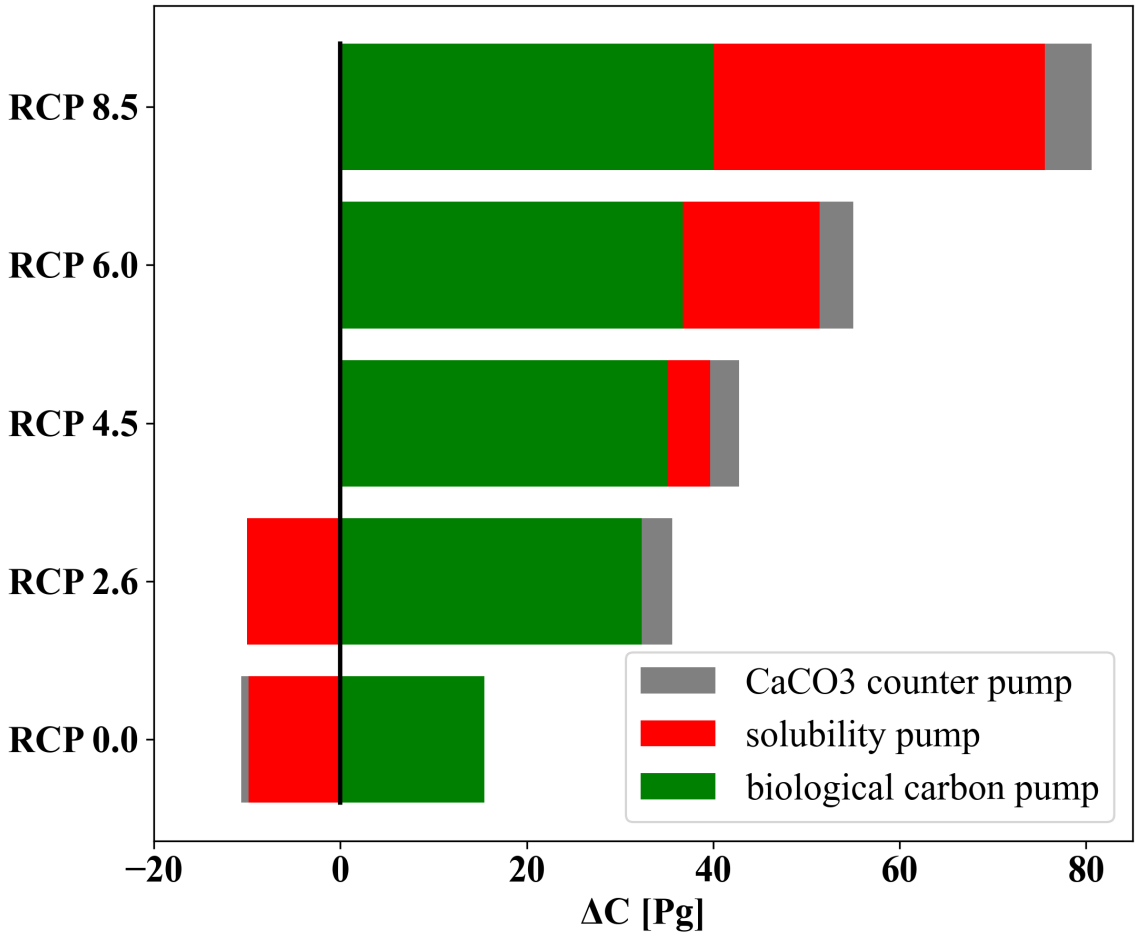

Figure S8. Cumulative global net increase in the ocean's carbon budget in the year 2100 after 80 years of pipe deployment (Pg C) via artificial upwelling divided into the individual contributions of the biological carbon pump (green), the solubility pump (red) and the $CaCO_3$ counter pump (grey; see also main text Discussion).

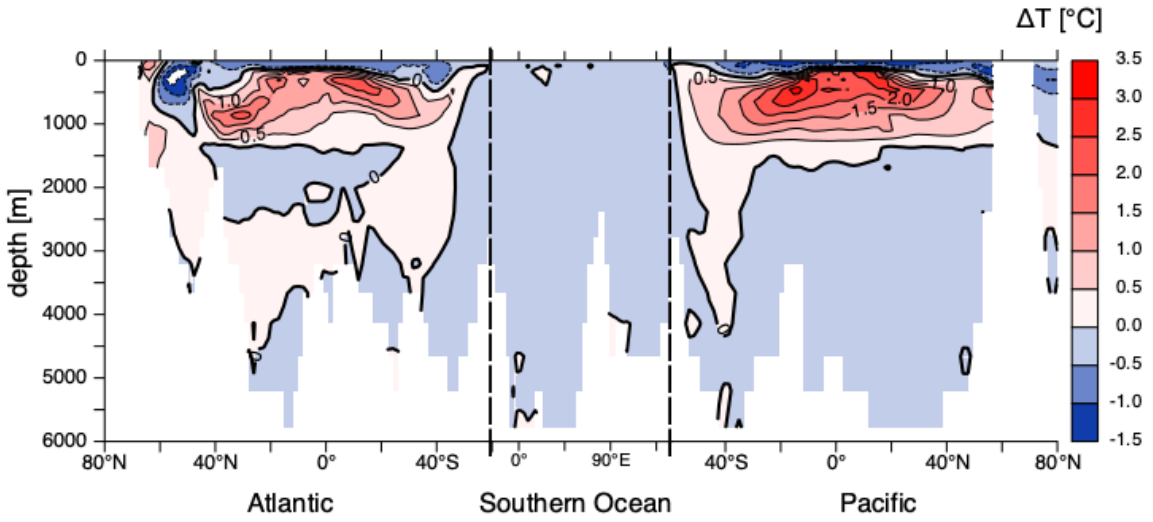

242

243 **Figure S9.** Temperature change (°C) between the experiments ArtUp_8.5 and REF_8.5
244 (ArtUp – Ref) in the year 2100 after 80 years of pipe deployment along an Atlantic
245 Ocean – Southern Ocean – Pacific Ocean transect.

246

247